A redshift survey between the clusters of galaxies A 548 and A 3367[*]

G. Andreuzzi[1,2]**, S. Bardelli**[3]**, R. Scaramella**[2]**, and E. Zucca**[4]

[1] Osservatorio Astronomico di Capodimonte, Via Moiariello 16, I-80131 Napoli, Italy
[2] Osservatorio Astronomico di Roma, Via Osservatorio 2, I-00040 Monteporzio Catone (RM), Italy
[3] Osservatorio Astronomico di Trieste, Via G.B. Tiepolo 11, I-34131 Trieste, Italy
[4] Osservatorio Astronomico di Bologna, Via Zamboni 33, I-40126 Bologna, Italy

Abstract. In this paper we present the results of a spectroscopic survey of galaxies in an area between the two clusters of galaxies A 548 and A 3367, suspected to be a close and interacting pair. With the use of multifiber spectroscopy, we measured 180 new velocities of galaxies in the central part of A 3367 and in the external regions of A 548.

The redshift histogram shows the presence of three velocity peaks, at $v \sim 12000$ km/s, $v \sim 30000$ km/s and $v \sim 40000$ km/s, respectively. For these we estimate the density excess, the mean velocity, and the velocity dispersion.

The first clump corresponds to an elongation of A 548: in particular we found a correspondence between the features of this peak and the substructures of A 548. The second peak has a velocity dispersion which is typical of clusters and the distribution of its members on the plane of the sky corresponds to the highest density peak in A 3367. We therefore suggest that the name A 3367 has to be attributed to this clump.

Our general conclusion is that, differently from expected, A 548 and A 3367 do not form a close pair of merging clusters, since the two structures are at significantly different redshifts. Moreover, we found that the complex dynamical structure of A 548 has large coherence, with a projected extension in the range of 1-3 h^{-1} Mpc.

Key words: galaxies: clusters: individual: A 548; A 3367 – galaxies: clusters: general – galaxies: distances and redshifts

1. Introduction

The determination of the galaxy distribution in clusters provides information on the status and the history of these structures through the study of their dynamics. Detailed studies spanning the entire range of morphologies of rich clusters of galaxies are important for understanding the formation and evolution of these systems. In a class of current cosmological models (e.g. cold dark matter dominated), rich clusters are formed hierarchically, by accretion of smaller subunits.

Several clusters are indeed known to present very lumpy morphologies (see e.g. Kriessler & Beers 1997 and references therein) revealing that these systems are in a merging process. The best studied examples are A2256 (Briel, Henry & Böhringer 1992), where a small group is detected in the X-ray band nearby the cluster center, and Coma, where a number of substructures are revealed (Biviano et al. 1996). Among the most spectacular cases are the encounters between clusters of similar richness, as for the A 3558 complex (Bardelli et al. 1994, 1996, 1998a, 1998b), where the dynamical processes reach unusual intensities, or the cluster A 3528, which is actually split into two merging X-ray emitting regions of similar properties (Schindler 1996).

The study of merging clusters is important because this process is thought to be responsible for a wide number of properties of the cluster galaxy population. Radio halos and relics of radiosources are found in clusters that visually present some degree of disturbance (Feretti & Giovannini 1996) and Burns et al. (1994) explained as a consequence of a merging event the presence of post-starburst galaxies in the large scale X–ray emitting filament connecting Coma with the NGC 4839 group.

A good starting point to individuate merging cluster candidates is that to extract close pairs from supercluster catalogues, as f.i. the list of Zucca et al. (1993), which reports groups of ACO clusters (Abell, Corwin & Olowin 1989) as a function of the density contrast. In this catalogue, the cluster pairs individuated by a density excess > 200 are very close systems, where often the nuclei are separated by less than one Abell radius (~ 1.5 h^{-1} Mpc, hereafter h=H_o/100): one of these pairs is formed by A 548 and A 3367.

The centers of the two clusters in the ACO catalog are separated on the plane of the sky by 77 arcmin, corresponding to ~ 2 h^{-1} Mpc at the distance of A 548. The separation in velocity was less clear: in fact the cluster A 548 is reported to have a mean velocity of $v = 12394$ km/s (determined on 133 redshifts, Davis et al. 1995), while A 3367 had reported a value of $v = 12780$ km/s (based on 6 velocities, Postman, Huchra & Geller 1992). However, Postman & Lauer (1995) reported a velocity of 13461 km/s for the brightest member of A 3367, clearly inconsistent with the above mean value.

The cluster A 548 [$\alpha(2000) = 05^h47^m00^s$; $\delta(2000) = -25^o36'00''$] is a cluster of richness class 1 and Bautz-Morgan type III. This cluster has been extensively studied both in the optical and X–ray wavelength. Davis et al. (1995) reported a global velocity dispersion of 903 km/s, but this cluster appears dynamically very complex. From the analysis of a mosaic of ROSAT PSPC observations, Davis et al. (1995) found the presence of three extended sources (dubbed S1, S2 and S3) with luminosities in the range $1.26 - 2.67 \times 10^{43}$ erg/s in the $[0.1 - 2.4]$ keV band. Performing a substructure analysis of the optical sample, they detected three subcondensations: two of these groups (labelled as a and b in their Table 4b) correspond to the extended X–ray emissions S1 and S2 respectively (see their Table 2). These optical subclumps were already found by Escalera et al. (1994) with the use of a wavelet decomposition analysis. They described A 548 as a binary cluster, when large spatial scales are considered. Moreover, they detected at smaller scales a central subgroup. These three components can be identified with the a, c and b substructures of Davis et al (1995), respectively. Another indication of the complex dynamical situation of this cluster appears from the different behaviour of galaxies with and without emission lines in their spectra: Biviano et al. (1997) in their analysis of the ENACS survey (Katgert et al. 1996, 1998) found a significant offset between the mean velocities of these two types of objects.

On the contrary, the cluster A 3367 was little studied so far. It has coordinates $\alpha(2000) = 05^h49^m40^s$; $\delta(2000) = -24^o28'00''$, is of richness class 0 and is classified as a Bautz-Morgan type I-II. No other relevant date was found in the literature apart the mean velocity reported above.

For these reasons we decided to concentrate our redshift survey on A 3367 and on the region between A 3367 and A 548, and in this paper we present a sample of 180 new radial velocities.

The paper is organized as follows: in Sect. 2 we present the sample and the data reduction, in Sect. 3 we discuss the dynamical properties of the three peaks found in the sample and finally in Sect. 4 we summarize our results.

2. The sample

2.1. The photometric catalogue

The starting photometric catalogue is the COSMOS/UKST galaxy catalogue of the southern sky (Yentis et al. 1992), obtained from automated scans of UKSTJ plates by the COSMOS machine. We extracted a circular region of 2° diameter, centered on $\alpha(2000) = 05^h48^m34^s$ and $\delta(2000) = -25^o17'27''$, containing 11525 objects to the limiting magnitude $b_J < 21.5$.

Fig. 1a shows the isodensity contours obtained binning the data in 2×2 arcmin cells and smoothing with a Gaussian of 6 arcmin of FWHM. For the two clusters circles of one Abell radius have been drawn around their nominal center. Note that it is already evident that A 548 is not a smooth cluster with a single central nucleus, but presents multiple condensations. Inside the Abell circle of A 3367 we note a single condensation
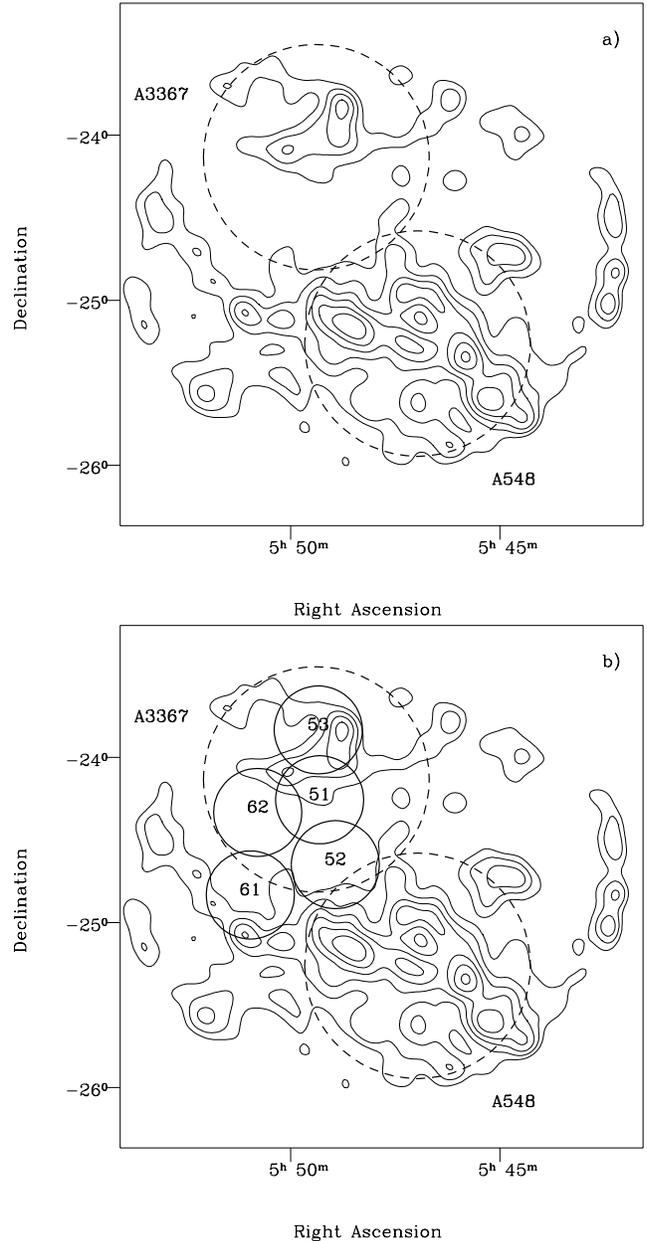

Fig. 1. a Isodensity contours of the region between A 548 and A 3367, centered on $\alpha(2000) = 05^h48^m34^s$ and $\delta(2000) = -25^o17'27''$. The data are binned in 2×2 arcmin cells and smoothed with a Gaussian of 6 arcmin of FWHM. For the two clusters, dashed circles of 1 Abell radius have been drawn. **b** As panel **a**, with the five OPTOPUS fields superimposed.

shifted northward with respect to the nominal center. In Fig. 1b the same isodensity contours are shown with superimposed the OPTOPUS fields positions.

The coordinates of the centers of these fields are listed in columns (2) and (3) of Table 1, together with the observation date in column (4).

Table 1. Observed OPTOPUS fields

FIELD	$\alpha(2000)$	$\delta(2000)$	Date
f51a	$05^h 49^m 24^s$	$-24°35'00''$	25/02/93
f51b	$05^h 49^m 24^s$	$-24°35'00''$	26/02/93
f52	$05^h 49^m 00^s$	$-25°00'00''$	25/02/93
f53	$05^h 49^m 24^s$	$-24°10'00''$	26/02/93
f61	$05^h 50^m 46^s$	$-25°09'47''$	16/10/93
f62	$05^h 50^m 46^s$	$-24°39'52''$	17/10/93

2.2. Observations

Spectroscopic measurements were obtained using the ESO 3.6m telescope at La Silla, equipped with the OPTOPUS multifiber spectrograph (Lund 1986), on the nights of 1993 February 25-26 and October 16-17.

The OPTOPUS multifiber spectrograph is formed by a bundle of 50 optical fibres at the Cassegrain focal plane of the telescope; this field has a diameter of 32 arcmin, and each fibre has a projected size on the sky of 2.5 arcsec. We used the ESO grating #15 with 300 lines/mm and a blaze angle of $4°18'$. This grating allows a dispersion of 174 Å/mm in our wavelength range (3700–6100) Å. We used the detector Tektronic 512×512 CCD with a pixel size of 27 μm, corresponding to 4.5 Å, i.e. a velocity bin of $\simeq 270$ km/s at 5000 Å; the resolution is ~ 12 Å. Four of the 50 fibres were dedicated to sky measurements, leaving 46 fibres available for the objects.

Fields f51a, f51b, f52 and f53 were observed for 1 hour, split into two half-hour exposures in order minimize the presence of cosmic hits. Fields f61 and f62 were observed only for 1/2 hour. The observing sequence was a 30-s exposure of a quartz halogen white lamp, a 60-s exposure of helium vapour lamp for fields f61 and f62, or 60-s exposure of helium + neon vapour lamp for fields f51, f52 and f53; then the scientific field, and again the arc and the white lamp.

2.3. Data reduction

The extraction of the one-dimensional spectra was performed using the APEXTRACT package as implemented in IRAF[1].

Positions and tracing solutions of lamps and objects were determined on the flat field exposures. The procedure we adopted to estimate the relative transmission of each fibre is based on the fitting of a Gaussian profile to the [OI]λ5577 sky line in each spectrum and on computing the continuum-subtracted flux of this line (Bardelli et al. 1994). If we assume that the flux and the shape of the spectrum of the night sky remain constant in the telescope field, this value is the same in each spectrum apart from the transmission of the fiber, which is a multiplicative factor. After having normalized the spectra, we can subtract the 'mean sky' obtained as the average of the 4 sky spectra.

---

[1] IRAF is distributed by the National Optical Astronomy Observatories, which is operated by AURA Inc. for the NSF.

2.4. Redshift data

We have obtained a total of 276 spectra: 45 were not useful for redshift determination (16% of the total), because of poor signal–to–noise ratio or badly connected fibers, and 51 turned out to be stars (22% of the reliable spectra), leaving us with 180 galaxy redshifts. The galaxies whose spectrum presents detectable emission lines are 79, corresponding to a percentage of 44% of the total.

The radial velocities of galaxies with spectra with absorption lines have been determined using the program XCSAO in the IRAF task RVSAO (Kurtz et al. 1992), which is based on the cross-correlation method of Tonry & Davis (1979). The determination of redshift is done by fitting a parabola to the main peak of the cross-correlation function. Sixteen different templates (eight stars and eight galaxies) were used for the determination of the radial velocities, choosing as better estimate the one which gave the minimum cross-correlation error, defined as:

$$\epsilon = \frac{3}{8} \frac{w}{(1+r)} \tag{1}$$

where w is the FWHM of the cross-correlation peak and r is the ratio between the height of the correlation peak and the rms of the antisymmetric part of the correlation function (Kurtz et al. 1992).

To estimate the redshift of spectra with strong emission lines we used the EMSAO program in the IRAF task RVSAO.

The top panel of Fig. 2 shows an example of a spectrum with strong emission features, with [OII]λ3727, [Hβ]λ4861, [OIII]λ4959, λ5007 lines, while in the bottom panel of Fig. 2 a spectrum with only absorption lines is presented.

In Tab. 2 - 7 we list the galaxies with redshift determination. Columns (1), (2) and (3) list the right ascension, the declination and the b_J magnitude respectively; column (4) and (5) give the heliocentric velocity ($v = cz$) and its internal error (in km/s), from absorption and emission lines respectively. The code in column (6) indicates the presence of emission lines: the symbols a, b, c, d, refer to [OII]λ3727Å, [Hβ]λ4861Å, [OIII]λ4959Å and [OIII]λ5007Å, respectively.

We remember that the cross-correlation errors are only internal formal errors. In order to have true statistical errors, these values have to be multiplied for the factor 1.53 found by Vettolani et al. (1998) comparing multiple observations of the same galaxies: after this correction, the average statistical error on our velocities is $\simeq 95$ km/s. If one wants to take into account also the uncertainties introduced by the different reduction procedures, the factor is slightly larger and has the value of ~ 1.9 (see Bardelli et al. 1994).

In order to check the zero point precision of our velocity scale, we considered the histogram of the measured velocities of the stars misclassified as galaxies (Fig. 3), which are expected to have a zero mean velocity. Considering only the 41 spectra with the higher signal-to-noise ratio, we found $< v >_{stars} = 22 \pm 14$ km/s ($\sigma_{stars} = 90$ km/s): this small systematic effect will be neglected in the following analysis, since the errors associated
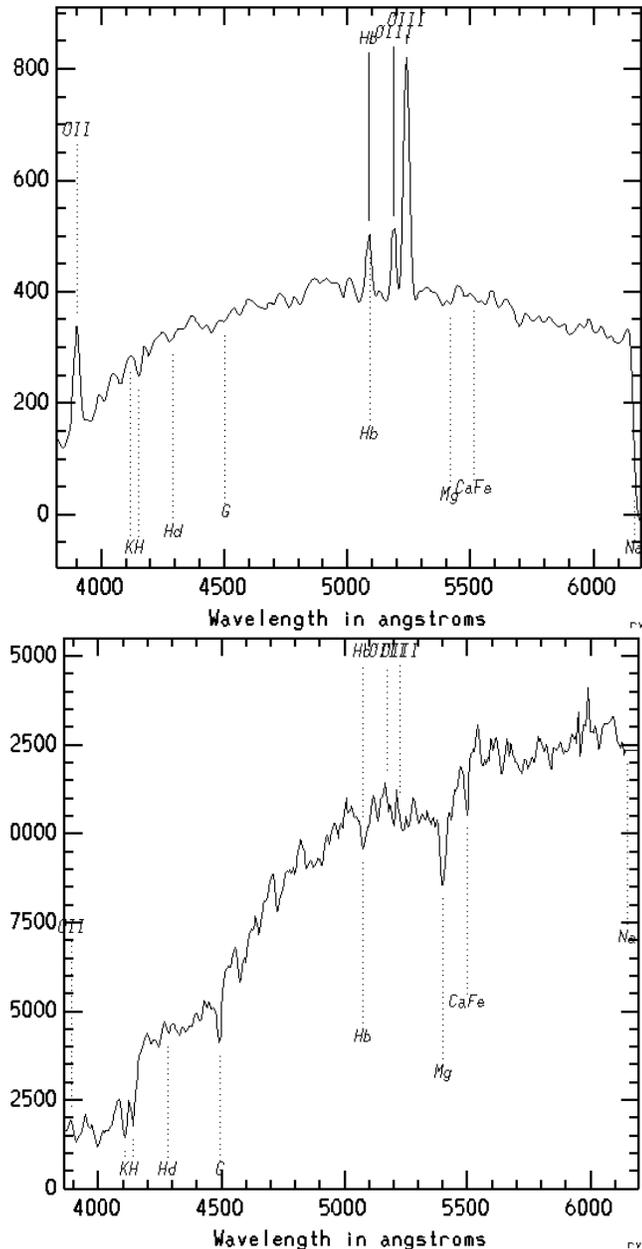
Fig. 2. Top: Example of a spectrum with strong emission lines ($v = 13954 \pm 29$ km/s). Bottom: Example of a spectrum with only features in absorption ($v = 13106 \pm 25$ km/s, $r = 17.5$). The spectra are plotted in arbitrary units on y-axis

Table 2. Field 51a

$\alpha(2000)$	$\delta(2000)$	b_J	v_{abs} km/s	v_{emis} km/s	notes
05 49 54.0	-24 23 19.9	15.8	13106±25		
05 49 27.0	-24 46 14.3	16.0	13367±48		
05 48 22.7	-24 33 15.1	18.2	30431±85		
05 49 22.2	-24 35 25.2	18.3	30771±38		
05 49 42.6	-24 41 47.2	17.5	13784±48		
05 49 41.1	-24 34 31.0	18.3	19647±25		
05 50 06.4	-24 23 40.7	17.9		13803±50	abcd
05 49 34.6	-24 30 57.2	16.6	19632±22		
05 49 07.6	-24 34 27.5	18.3	30596±26		
05 49 39.7	-24 25 26.3	16.0		12237±53	abcd
05 49 59.8	-24 28 05.9	19.0		30797±33	abcd
05 49 41.3	-24 32 42.9	15.7	13363±29		
05 48 26.6	-24 42 09.9	17.3	13363±20		
05 49 36.3	-24 30 18.9	18.7	19837±49		
05 48 25.5	-24 41 43.9	18.8		13954±29	abcd
05 49 50.8	-24 39 55.1	16.9	13289±32		
05 48 48.6	-24 22 42.6	14.9	11895±51		
05 49 10.2	-24 38 22.8	18.6	42066±63		
05 48 23.1	-24 32 32.8	17.7	30261±70		
05 49 37.5	-24 32 10.5	18.5		42783±179	abcd
05 48 25.5	-24 43 15.1	18.1		13950±22	abcd
05 50 17.9	-24 28 38.1	17.5		11891±36	ad
05 49 37.4	-24 33 33.2	17.9	19913±21		
05 48 50.2	-24 21 06.9	16.2	13741±30		
05 49 39.5	-24 39 08.2	18.8	39649±105		
05 49 26.1	-24 22 25.5	17.4	19498±20		
05 48 37.0	-24 26 36.8	18.6	42688±62		
05 49 14.8	-24 25 52.1	17.8		13447±59	bcd
05 48 22.1	-24 41 43.7	16.8	13706±77		
05 50 12.8	-24 40 08.6	18.9		41774±15	abcd
05 49 41.2	-24 34 06.4	18.1	11803±60		
05 48 48.7	-24 29 46.0	18.6	30758±28		
05 49 53.8	-24 27 58.7	16.6	13923±110		
05 49 20.2	-24 38 39.2	18.6	13684±136		
05 48 42.0	-24 26 50.3	18.7		12119±69	abd
05 50 05.1	-24 28 47.5	16.5	12131±50		
05 49 12.2	-24 29 59.5	18.7	51690±52		
05 49 04.5	-24 29 01.0	17.5	13529±112		
05 50 03.6	-24 38 14.1	15.0	13368±26		

estimate of this effect, although with a smaller sample. On the basis of 10 galaxies, we find $< v_{abs} - v_{emiss} >= 60 \pm 30$ km/s, consistent within the errors with the result of Cappi et al. (1998).

3. Discussion

In Fig. 4a the histogram of the galaxy velocities is shown. There are at least three peaks (labelled as A, B, C in the figure): the first is at a velocity of ~ 13000 km/s, the second and the third at ~ 30000 km/s and ~ 40000 km/s, respectively. Peak A is at the same velocity as A 548 and presents a clear bimodality.

Although no significant differences (through a K-S test) are found between the overall distributions of galaxies with and without emission lines, a more detailed analysis of the three peaks reveals that the two distributions inside the single peaks are in fact different (see Fig.4b). In particular, for peak A a separation in velocity is evident, as the population of emission line objects is dominant in the clump at lower velocity: the percentage of emission line galaxies with respect to the total in this clump is 54%, while it is 39% in the higher velocity clump. Because galaxies with and without emission lines have different luminosity functions (Zucca et al. 1997), it could be suspected that their different distribution is a consequence of a change

to the galaxy velocities are larger. However, we cannot exclude that the value of $< v >_{stars}$ is completely due to bulk motions of stars in this region of the sky.

Very recently, Cappi et al. (1998), analysing the ESP survey (Vettolani et al. 1997, 1998), noted a systematic difference between the velocities estimated from the emission lines and the cross-correlation for the same galaxy, with an average difference of $< v_{abs} - v_{emiss} >= 93 \pm 6$ km/s (obtained from about 750 galaxies). Our observations are taken in the same instrumental configuration of the ESP survey and can give an independent

Table 3. Field 51b

α(2000)	δ(2000)	b_J	v_{abs} km/s	v_{emis} km/s	notes
05 49 08.5	-24 36 49.2	20.0	53764±36		
05 49 16.7	-24 38 47.7	20.1	42217±36		
05 48 24.8	-24 34 23.8	20.1	30341±55		
05 50 03.6	-24 48 00.9	20.1		41842±69	acd
05 49 08.4	-24 44 27.7	19.6		30031±27	acd
05 50 16.0	-24 26 50.6	20.1		53060±80	a
05 49 03.4	-24 19 56.0	19.8		80128±80	a
05 50 33.7	-24 35 35.7	19.6		41023±77	abcd
05 48 47.0	-24 24 14.5	19.9		40152±50	ab
05 49 48.0	-24 26 13.0	20.1		17267±85	c
05 49 29.1	-24 21 22.5	20.1	19508±69		
05 50 01.6	-24 37 33.2	19.7		13274±77	abcd
05 48 45.4	-24 22 12.6	19.9		66537±80	a
05 49 58.5	-24 39 02.4	20.0		19932±17	acd
05 48 56.5	-24 26 15.2	19.8		88903±80	a
05 49 30.9	-24 33 17.8	20.2		65483±28	abcd
05 48 36.6	-24 46 25.4	19.8	50943±120		
05 50 33.0	-24 34 18.7	20.0		34930±22	ab
05 48 38.1	-24 25 11.6	19.8	31182±72		
05 50 19.4	-24 38 06.4	19.9	86756±84		
05 49 58.0	-24 29 21.7	20.0	81631±75	81612±80	a
05 48 51.7	-24 21 40.5	19.7	66526±91	66285±80	a
05 48 49.4	-24 21 49.2	19.7		13598±56	abcd
05 49 42.0	-24 21 14.7	20.0	66954±52		
05 49 39.0	-24 23 46.6	19.8	51356±62		

Fig. 3. Histogram of the velocities of 41 stars observed by chance in our survey. The superimposed solid curve corresponds to a Gaussian with $< v >= 22$ km/s and $\sigma = 90$ km/s.

Table 4. Field 52

α(2000)	δ(2000)	b_J	v_{abs} km/s	v_{emis} km/s	notes
05 49 10.9	-24 53 17.3	17.5	19748±47		
05 49 08.9	-25 13 50.5	19.8	13679±106		
05 49 36.2	-24 51 09.5	17.3		13394±51	abcd
05 48 26.3	-25 12 47.1	17.2	11039±105		
05 48 48.2	-25 11 48.8	18.9		11949±84	acd
05 48 36.7	-24 54 18.4	19.1	50873±86		
05 49 24.5	-25 02 09.4	19.1		30093±58	acd
05 49 33.7	-25 07 09.6	18.3	16959±81	16890±49	acd
05 49 54.5	-25 03 54.6	18.9	12048±131		
05 49 29.6	-25 00 53.2	18.0	13255±120		
05 49 55.1	-24 56 55.4	18.0	13449±93		
05 49 34.4	-25 04 33.3	16.9	14350±33		
05 49 15.3	-25 07 57.7	19.2	11727±104		
05 48 36.3	-25 01 19.1	19.7	50542±67		
05 48 37.5	-24 53 33.6	18.8		30361±26	abcd
05 48 35.9	-25 10 09.7	18.8	22404±35		
05 48 22.7	-25 12 17.0	18.1	13187±25		
05 49 22.9	-24 58 50.4	19.5		12721±41	ad
05 48 41.1	-25 09 13.4	18.0	12332±91		
05 48 58.5	-25 06 08.5	19.7		22400±73	abcd
05 50 01.2	-24 53 29.7	17.6	13521±93		
05 48 04.8	-24 57 34.5	19.4		52703±124	abcd
05 49 09.5	-25 03 22.5	19.3		12213±54	abd
05 48 30.0	-24 50 20.6	18.9		11886±100	ac
05 48 14.5	-25 07 54.8	19.6		37211±150	ad
05 48 58.5	-24 49 56.1	19.4		29678±129	abcd
05 48 47.0	-25 09 16.8	18.6		13229±66	ac
05 49 40.6	-25 06 27.5	18.3	48574±72		
05 49 18.6	-25 15 22.1	19.6	12320±95		
05 49 23.6	-25 03 36.1	19.7		27429±58	ac
05 48 40.0	-24 59 20.0	17.0	13523±55		
05 49 40.8	-25 10 56.0	19.8		114834±80	a
05 48 30.3	-24 52 08.8	19.8		13229±58	abcd
05 48 02.5	-25 01 20.5	16.2		12018±131	ac

Table 5. Field 53

α(2000)	δ(2000)	b_J	v_{abs} km/s	v_{emis} km/s	notes
05 49 05.5	-24 06 43.5	19.3	31145±31		
05 48 49.2	-24 15 18.8	17.6	29392±39		
05 50 30.9	-24 05 50.7	19.1	30655±30		
05 48 51.6	-24 06 45.8	19.3	30283±36		
05 48 55.1	-24 13 17.0	18.8	31518±31		
05 49 15.7	-24 01 41.6	18.9		13810±56	ad
05 49 20.8	-24 03 49.8	17.1	30057±61		
05 48 53.5	-24 02 07.2	19.4	30506±96		
05 48 47.5	-24 10 52.4	20.6	30588±36		
05 48 49.4	-24 09 12.6	19.4	31078±42		
05 49 26.7	-24 17 06.9	17.8	29254±79		
05 49 04.8	-24 04 29.3	16.0	13618±59		
05 49 55.3	-24 05 31.2	18.1		30080±73	abcd
05 49 17.3	-24 18 31.9	19.3		77349±27	ab
05 48 45.9	-24 13 33.4	19.1	31014±49		
05 50 03.0	-24 01 20.0	16.5	8981±84	8917±15	abcd
05 50 20.7	-24 16 15.4	19.4	42073±63		
05 49 55.3	-24 08 03.3	19.2		30121±23	abcd
05 48 38.1	-24 20 42.8	19.4	31206±29		
05 49 13.4	-24 02 46.0	19.3	93404±60		
05 48 50.8	-24 20 21.1	16.5	19944±25		
05 48 58.1	-24 05 06.7	18.8	30472±28		
05 48 57.5	-24 17 25.1	18.1	31429±43		
05 50 29.7	-24 12 45.1	19.1		13870±37	abcd
05 48 41.2	-24 15 01.2	18.1	30736±32		
05 48 36.8	-24 07 04.5	19.0	31040±71		
05 49 02.0	-24 18 06.2	17.1		13120±65	abd
05 49 17.8	-23 56 52.7	19.5	29940±39		
05 49 07.7	-24 09 30.9	18.9	3024±238		
05 48 57.0	-24 09 53.4	17.5	29551±112	29345±111	ad
05 49 25.1	-24 03 23.5	18.7	42086±69	42136±80	a
05 49 43.9	-24 10 55.1	18.3	31847±110		
05 49 01.7	-24 04 44.3	18.3	30776±33		

in the relative values of their selection functions: however, the width of peak A is relatively narrow (less than 1000 km/s) and therefore this effect is more likely due to a real variation in morphological composition in the two subclumps.

We estimated the dynamical parameters (mean velocity and velocity dispersion) of the three peaks with the biweight estimators of location and scale (Beers et al. 1990). The advantage of these estimators, with respect to the standard mean and dispersion, is that of minimizing biases from interlopers, giving less

Table 6. Field 61

α(2000)	δ(2000)	b_J	v_{abs} km/s	v_{emis} km/s	notes
05 51 23.0	-25 23 13.8	15.9	42806±44		
05 50 15.9	-25 16 15.4	19.0	11696±68		
05 51 28.1	-25 24 16.9	18.3	40426±92	40383±80	a
05 51 23.7	-25 24 59.0	19.9	41583±98		
05 50 22.3	-25 18 09.2	17.2	11595±28		
05 51 18.0	-25 15 40.8	17.9		12124±40	abcd
05 51 55.3	-25 14 14.2	19.6		44811±20	ad
05 50 01.8	-25 18 49.2	19.1		11779±62	acd
05 51 07.9	-25 09 31.7	17.9		11769±73	abcd
05 52 04.2	-25 12 22.5	19.7	45116±112		
05 51 52.9	-25 12 16.1	19.2	45788±66		
05 50 13.7	-25 20 11.6	19.6	30356±58		
05 50 57.1	-25 01 13.6	17.0	26279±53	26228±35	bcd
05 51 16.6	-25 19 45.4	19.6	42172±61		
05 50 17.0	-24 58 37.4	19.9		17715±106	ad
05 50 14.2	-25 13 55.0	18.2	11739±69		
05 51 13.2	-25 24 22.3	18.7		11652±45	abcd
05 50 47.1	-25 04 50.3	20.6	26277±82		
05 50 41.0	-25 03 56.6	19.3		59525±80	a
05 51 14.9	-25 24 57.3	19.6		17674±123	abcd
05 50 15.6	-25 10 02.8	18.7		29035±34	abcd
05 50 42.0	-25 20 04.4	19.7	61220±56		
05 51 19.9	-25 12 19.8	19.1		44958±80	a
05 51 46.0	-25 18 32.5	17.7	13427±87	13428±86	a
05 50 31.0	-25 01 34.4	18.5		11811±52	ad
05 51 28.4	-25 18 49.0	19.8		46585±96	ab
05 49 59.7	-25 12 48.1	19.3		16948±68	abcd
05 50 17.3	-25 02 05.4	18.3	40337±35		
05 50 58.0	-24 56 24.2	17.4	29049±51		
05 50 01.8	-25 08 04.5	19.7		12402±132	a
05 52 03.1	-25 03 22.1	17.2	41200±105		
05 50 46.0	-25 15 40.7	17.7	11883±64		
05 51 31.6	-25 23 24.6	19.4	41210±44		

Table 7. Field 62

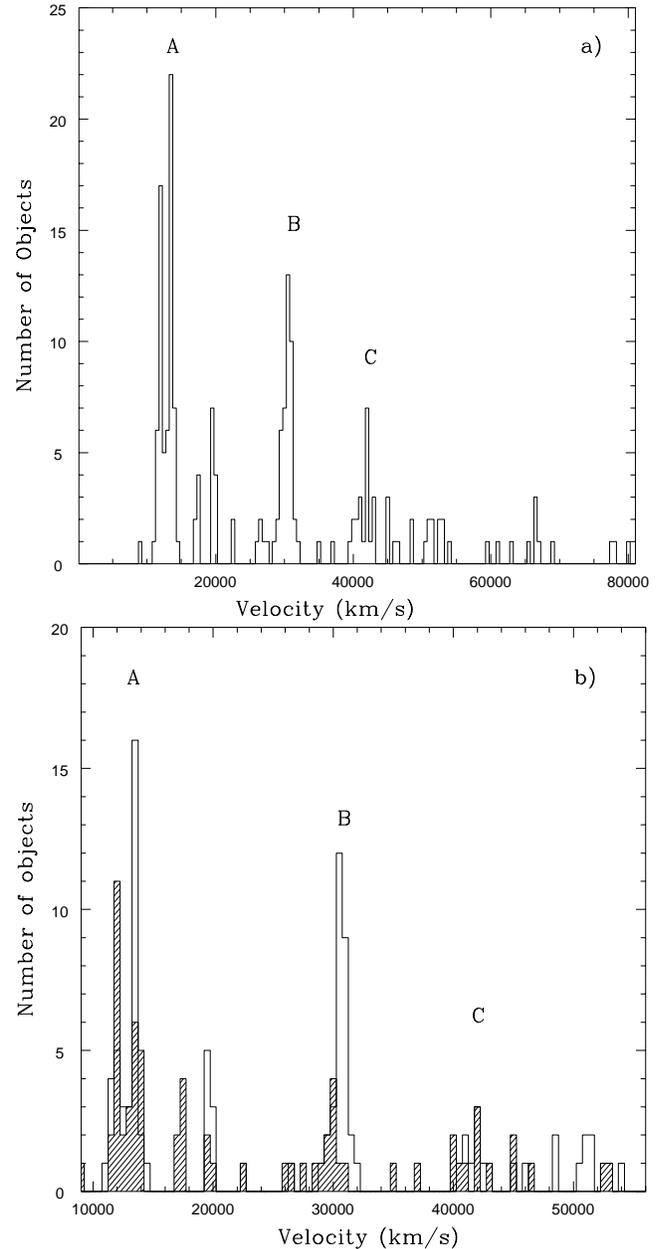| α(2000)	δ(2000)	b_J	v_{abs} km/s	v_{emis} km/s	notes
05 50 39.5	-24 28 33.7	19.7	52479±121		
05 50 56.6	-24 34 45.0	17.8		11417±39	abcd
05 51 38.5	-24 31 02.5	17.5	13219±28		
05 51 01.0	-24 38 24.4	18.9		13594±65	ad
05 51 20.3	-24 40 20.0	20.0	53185±91		
05 50 20.8	-24 48 31.4	18.9	48556±78		
05 50 17.3	-24 52 30.0	20.0		19575±17	abd
05 50 51.9	-24 52 28.2	19.2		19535±31	abcd
05 51 36.5	-24 46 04.5	20.2		26141±90	ad
05 51 46.5	-24 35 31.4	18.1	28357±61	28398±76	a
05 51 02.5	-24 46 20.4	18.8	30549±47		
05 50 30.0	-24 30 50.5	20.3		40183±60	abcd
05 50 13.7	-24 51 10.4	20.0		69130±80	a
05 51 01.4	-24 49 48.0	20.3		66474±80	a
05 51 03.1	-24 54 17.2	18.7		17724±80	a
05 50 38.3	-24 24 58.4	20.1	88022±98		

Fig. 4. **a** Histogram of the observed velocities in bins of 500 km/s for all galaxies of our sample. **b** Close up of panel **a**; the shadowed histogram represents the distribution of galaxies with emission lines, while the open histogram refers to the galaxies with only absorption lines.

weight to data with higher distance from the median. The confidence intervals of the two estimators are calculated boostrapping the data with 100 random catalogs. In order to find the velocity range in which the cluster members lie, we have assumed that the velocity distribution of cluster galaxies is Gaussian, as expected when the system has undergone a violent relaxation (see details in Bardelli et al. 1994).

For the case of peak A, in which the presence of a substructure was suspected on the basis of both a visual inspection of the velocity histogram and the shape estimators a, b_1, b_2 and I (see Bird & Beers 1993), we checked if the distribution is consistent with a single Gaussian or if it is bimodal applying the KMM test (Ashman et al. 1994), using the program kindly provided by the authors. This test gives the likelihood ratio between the hypothesis that the dataset is better described by the sum of two Gaussians and the null hypothesis that the dataset is better described by a single Gaussian.

In Table 8, we report the dynamical parameters for the velocity excesses found in our sample (see the discussion below). Column (1) refers to the peak identification, column (2) reports the number of velocities used, columns (3) and (4) are the estimated mean velocity and velocity dispersion.

Table 8. Estimated dynamical parameters

Peak	N	$< v >$(km/s)	σ (km/s)
Peak A	64	12866 ± 150	869 ± 78
Clump 1	28	11951 ± 116	267 ± 59
Clump 2	36	13498 ± 111	260 ± 52
Peak B	40	30477 ± 107	602 ± 148
Peak C	17	41603 ± 215	849 ± 217
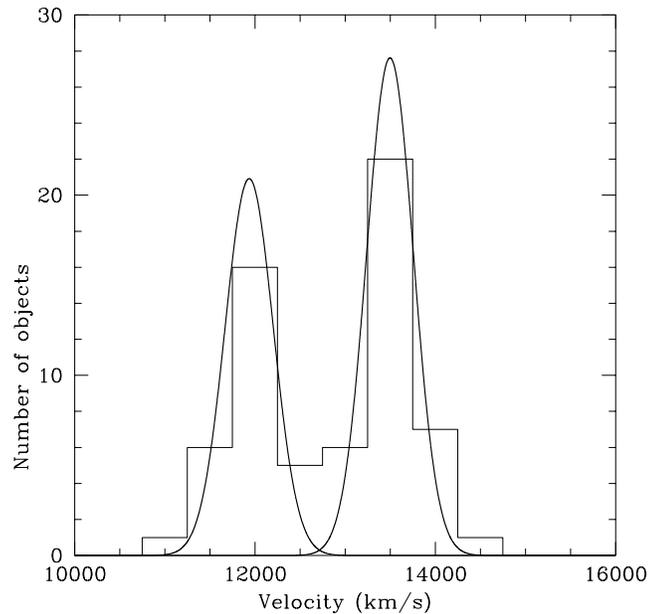
Fig. 5. Velocity distribution of galaxies belonging to peak A with superimposed the two Gaussians with $< v >_1 = 11951$ km/s and $\sigma_1 = 267$ km/s and $< v >_2 = 13498$ km/s and $\sigma_2 = 260$ km/s. Among the 64 objects of the peak, 28 have been assigned to the lower velocity group and 36 to the higher velocity one.

3.1. Peak A

Peak A, formed by 64 galaxies, is at the same velocity as A 548 and has $< v >= 12866 \pm 150$ km/s and $\sigma = 869 \pm 78$ km/s. The shape estimators a and b_2 revealed a significant deviation from the null hypothesis of Gaussianity (at more than 95% significance level). The KMM test revealed that the distribution is significantly better described by two Gaussians, both in the homoscedastic and in the heteroscedastic case. Assigning the objects to the two groups on the basis of the *a posteriori* probability given by the KMM algorithm (see Ashman et al. 1994) and estimating the dynamical parameters with the biweight estimators, we found $< v >_1 = 11951 \pm 116$ km/s and $\sigma_1 = 267 \pm 59$ km/s (based on 28 velocities) and $< v >_2 = 13498 \pm 111$ km/s and $\sigma_2 = 260 \pm 52$ km/s (based on 36 objects). Fig. 5 shows a close up of the velocity distribution of galaxies in peak A, with superimposed the two Gaussians of parameters $< v >_1$, σ_1 and $< v >_2$, σ_2. No significant differences are found, inside each clump of peak A, between the dynamical parameters of galaxies with and without emission lines.
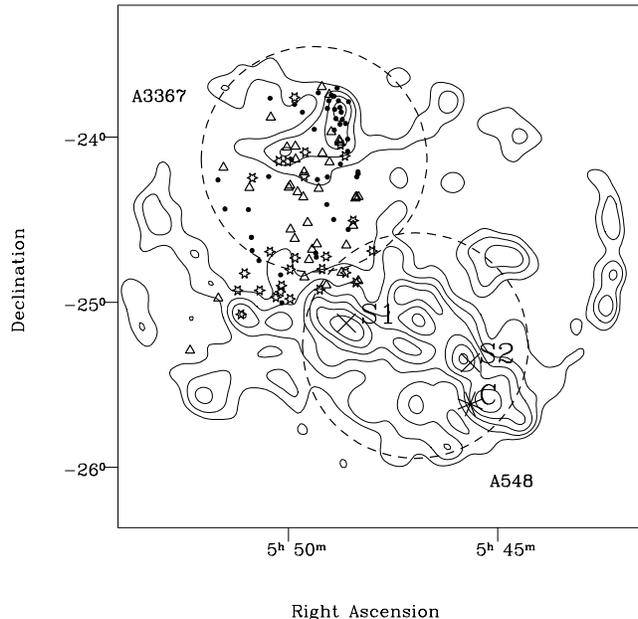

Fig. 6. Positions of galaxies with $10000 < v < 12700$ km/s (stars), with $12700 < v < 15000$ km/s (triangles) and $25000 < v < 35000$ km/s (black dots). Crosses refer to the positions of X–ray extended sources and the asterisk refers to the position of an optical substructure in A 548 (see Davis et al. 1995).

These mean velocities can be compared with those of the subclumps found by Davis et al. (1995) in A 548. Our value of $< v >_1$ is well consistent with their Clump a (see their Table 4b). Our $< v >_2$ is $2.6\,\sigma$ different from the mean velocity of their Clump b: however assuming that the error on the Davis et al. determination (not reported in their paper) could be similar to ours, the discrepancy may be reduced to less than $1\,\sigma$. Moreover, our values are well in agreement with those reported by Escalera et al. (1994).

More noticeable is the difference in the velocity dispersions. Clumps a and b have values of 638 km/s and 553 km/s respectively, while we estimated ~ 260 km/s for both groups. This fact could be an indication of a dependence of the velocity dispersion on the distance from the group centers.

The dynamical situation of peak A is therefore very similar to that of A 548 and this peak has to be considered an extension of the nearby cluster rather than a separated entity. In particular, the subcondensation of peak A at lower velocity is part of Clump a, while the higher velocity group of peak A is associable to Clump b.

In order to see the relative distance of the clumps detected in A 548 from our galaxies, we plotted on the isodensity contours the positions of their centers and the distribution on the sky of our sample. In Fig. 6 stars represent galaxies with $10000 < v < 12700$ km/s and triangles refer to objects with $12700 < v < 15000$ km/s. The big crosses are the reported centers of the extended emissions found in the ROSAT observations labelled as S1 and S2 in Table 2 of Davis et al. and coincident with their optical Clumps a and b. Their source S3 falls outside the figure.

We reported also the position of their Clump c as an asterisk. Note the good coincidence between these positions and peaks in the density field.

The extension in A 3367 of Clump a of Davis et al. seems to have two condensations (see stars in Fig. 6) at $\alpha(2000) \sim 05^h50^m$, $\delta(2000) \sim -24^o10'$ and $\alpha(2000) \sim 05^h50^m$, $\delta(2000) \sim -25^o00'$, at the distances of ~ 65 and ~ 30 arcmin from the corresponding substructure in A 548, respectively.

The extension in A 3367 of Clump b (see triangles in Fig. 6) is more smooth and spans all the distances between 1° and 1.5^o from its center, corresponding to ~ 2-3 h^{-1} Mpc.

Finally we note that the mean velocity reported by Postman et al. (1992) for A 3367 is consistent with the redshift of peak A. The velocity of the brightest cluster member (Postman & Lauer 1995) reveals that this galaxy is part of the higher velocity clump of peak A: therefore this galaxy is probably associated to A 548 rather than to A 3367.

3.2. Peaks B and C

The estimated dynamical parameters of the second peak seen in the redshift histogram are $< v > = 30477 \pm 107$ km/s and $\sigma = 602 \pm 148$ km/s, based on 40 velocities. The percentage of emission line galaxies is 25%. In Fig. 6, the objects belonging to this structure are plotted as black dots and seem to be concentrated around a density peak at $\alpha(2000) \sim 05^h48^m$ and $\delta(2000) \sim -23^o50'$. The shape estimators indicate that the distribution is consistent with a Gaussian. Given the fact that this density excess is the largest one inside one Abell radius from the nominal center of A 3367 and considering that its velocity dispersion is typical of a cluster, we suggest that the name A 3367 should be attributed to peak B.

Finally, the estimated mean velocity and velocity dispersion for peak C are $< v > = 41603 \pm 215$ km/s and $\sigma = 849 \pm 217$ km/s, determined with 17 objects. The Gaussianity of the distribution cannot be excluded.

4. Summary

We have presented the results of a redshift survey in an area between the Abell clusters A 548 and A 3367. These two clusters have been suspected to be a close pair and therefore candidates to undergo a merging process.

We obtained 180 new galaxy velocities with the use of multifiber spectroscopy, 44% of which presents emission lines. The redshift histogram shows clearly three peaks at $v \sim 12000$ km/s, $v \sim 30000$ km/s and $v \sim 40000$ km/s: for each of them we have estimated the dynamical parameters.

The first structure (peak A) is at the velocity of A 548 and could be considered as an extension of this cluster. In particular, this peak is formed by two substructures, corresponding to two subclusters in A 548 revealed by Davis et al. (1995) both in the optical distribution of galaxies and in a ROSAT X-ray map. The velocity dispersions of our two clumps in peak A are significantly smaller than those determined in the subclumps of Davis et al., while the mean velocities are in agreement.

Peak B has $< v > = 30477$ km/s and a velocity dispersion of ~ 600 km/s; the distribution of its members on the plane of the sky corresponds to the highest density excess of A 3367: for this reason we suggest that the name A 3367 should be attributed to this clump. The mean velocity reported for A 3367 by Postman et al. (1992) is based on galaxies belonging to peak A, and therefore to an extension of A 548 rather than to A 3367.

Our general conclusion is that A 548 and A 3367 is not a close pair of merging clusters, as the two structures have a significantly different redshift. However, we found that the complex dynamical structure of A 548 has large coherence, with a projected extension in the range of 1-3 h^{-1} Mpc.

References

Abell, G.O., Corwin, H.G., Olowin, R.P., 1989, ApJSS 70, 1 [ACO]

Ashman, K.M., Bird, C.M., 1994, AJ 108, 2348

Bardelli, S., Zucca, E., Vettolani, G. et al., 1994, MNRAS 267, 665

Bardelli, S., Zucca, E., Malizia, A. et al., 1996, A&A 305, 435

Bardelli, S., Zucca, E., Zamorani, G., Vettolani, G., Scaramella, R., 1998a, MNRAS 296, 699

Bardelli, S., Pisani, A., Ramella, M., Zucca, E., Zamorani, G., 1998b, MNRAS in press

Beers, T.C., Flynn, K., Gebhart, K., 1990, AJ 100, 32

Bird, C.M., Beers, T.C., 1993, AJ 105, 1596

Biviano, A., Durret, F., Gerbal, D. et al., 1996, A&ASS 111, 265

Biviano, A., Katgert, P., Mazure, A. et al., 1997, A&A 321, 84

Briel, U., Henry, J.P., Böhringer, H., 1992, A&A 259, L1

Burns, J.O., Roettiger, K., Ledlow, M., Klypin, A., 1994, ApJ 427, L87

Cappi, A., et al., 1998, A&A in press

Davis, D.S., Bird, C.M., Mushotzky, R.F., Odewahn, S.C., 1995, ApJ 440, 48

Escalera, E., Biviano, A., Girardi, M., et al., 1994, ApJ 423, 539

Feretti, L., Giovannini, G., 1996, in Extragalactic Radio Sources, IAU Symp. 175, R. Fanti, Fanti, C., Ekers, R., Padrielli, L., eds, Kluwer Ac. Publ., p.333

Katgert, P., et al., 1996, A&A 310, 8

Katgert, P., Mazure, A., den Hartog, et al., 1998, A&ASS 129, 399

Kriessler, J.R., Beers, T.C., 1997, AJ 113, 80

Kurtz, M.J., Mink, D.J., Wyatt, W.F. et al. 1992, in Astronomical Data Analysis Software and Systems I, Worrall, D.M., Biemesderfer, C., and Barnes, J., eds., ASP conference series vol.25 p.432

Lund, G., 1986, OPTOPUS-ESO operating manual N.6

Postman, M., Huchra, J.P., Geller, M.J., 1992, ApJ 384, 404

Postman, M., Lauer, T.R., 1995, ApJ 440, 28

Schindler, S., 1996, MNRAS 280, 309

Tonry, J., Davis, M., 1979, AJ 84, 1511

Vettolani, G., et al., 1997, A&A 325, 954

Vettolani, G., et al., 1998, A&ASS in press

Yentis, D.J., Cruddace, R.G., Gursky, H. et al., 1992, in Digitized Optical Sky Surveys, MacGillivray, H.T. & Thomson, E.B. eds., Kluwer, Dordrecht, p. 67

Zucca, E., Zamorani, G., Scaramella, R., Vettolani, G., 1993, ApJ 407, 470

Zucca, E., et al., 1997, A&A 326, 477